Slow light using semiconductor quantum dots

2004 J. Phys.: Condens. Matter 16 S3727

(http://iopscience.iop.org/0953-8984/16/35/014)

INSTITUTE OF PHYSICS PUBLISHING JOURNAL OF PHYSICS: CONDENSED MATTER

J. Phys.: Condens. Matter **16** (2004) S3727–S3735 PII: S0953-8984(04)83269-7

Slow light using semiconductor quantum dots

J Kim[1], S L Chuang[1], P C Ku[2] and C J Chang-Hasnain[2]

[1] Department of Electrical and Computer Engineering, University of Illinois at Urbana-Champaign, 1406 W. Green Street, Urbana, IL 61801, USA
[2] Department of Electrical Engineering and Computer Science, University of California at Berkeley, 175M Cory Hall, Berkeley, CA 94720, USA

E-mail: s-chuang@uiuc.edu

Received 6 July 2004
Published 20 August 2004
Online at stacks.iop.org/JPhysCM/16/S3727
doi:10.1088/0953-8984/16/35/014

Abstract

A variable semiconductor optical buffer based on the electromagnetically induced transparency in a quantum dot waveguide is theoretically investigated with feasible parameters for applications to a 40 Gbps optical network. We show the refractive index and absorption spectra of the quantum dot waveguide at various pump levels, which exhibit an optimal pump power for maximum slow-down factor, in agreement with the previous experimental observation using a Pr-doped solid. The group velocity slow-down factor is theoretically analysed as a function of the pump intensity at different broadened linewidths. Inhomogeneous broadening in self-assembled quantum dots degrades the slow-down factor. In order to reduce the inhomogeneous broadening effects, we propose to use a resonant microcavity structure with quantum dots embedded in the active layer to enhance the slow-down factor.

(Some figures in this article are in colour only in the electronic version)

1. Introduction

Variable optical buffers are one of the crucial components in the implementation of optical signal processing and all-optical packet-switched networks. In such a buffer, data would be kept in the optical domain throughout the storage time without being converted into the electronic domain. The buffer must be able to turn on to store and off to release optical data at a very rapid rate by an external command. The fibre optical delay line is widely used but it lacks the functionality of variable time delay due to the fixed nature of the fibre length. There are several other possible ideas of implementing a variable optical delay line such as electromagnetically induced transparency (EIT) [1–3], Moiré grating [4], and recirculating fibre loop [5]. Experimental results of a slow-down factor of 10^7 have been reported using the EIT mechanism in a gas cell at 350 K [6] and in a Pr:doped solid at 5 K [7]. However, in this

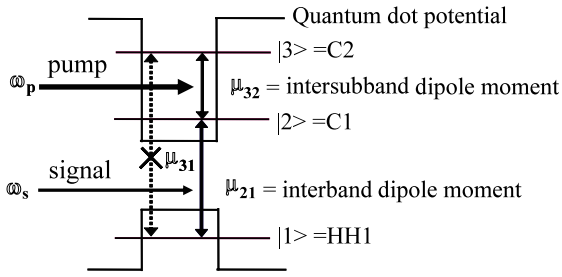

Figure 1. Schematic diagram of the potential profiles and relevant parameters in a semiconductor quantum-dot system for the electromagnetically induced transparency (EIT) operation. (HH1 = the heavy-hole ground state, C1 = the conduction band ground state, and C2 = the first excited state of conduction band.)

case the transmission bandwidth of the group velocity slow down is tens of kilohertz, which is not suitable for optical buffer applications [7]. Recently, a semiconductor optical buffer using EIT in a quantum dot (QD) medium has been proposed and its performance of slow light was theoretically predicted [3]. We investigate the performance of the proposed semiconductor optical buffer for application to 40 Gbps optical communication systems. We use feasible parameters of strained QDs from our band structure model as well as published experimental data on linewidths.

In the formation of self-assembled QDs, inhomogeneous broadening exists due to the nonuniformity of size, strain distribution, and material composition of QDs [8]. This nonuniformity makes the signal and pump beams experience different detunings at different QDs. The slow-down factor induced by the misaligned QDs can even be negative at the signal wavelength, cancelling the positive slow-down factor generated by the aligned QDs [9]. Eventually, this inhomogeneous broadening of QDs reduces the slow-down factor and contributes to signal distortion. In order to alleviate degradation effects induced by inhomogeneous broadening, a multicolour pumping scheme was proposed [9]. In this paper, we propose to put a small number of quantum dots in a resonant microcavity to overcome the deleterious effect of inhomogeneous broadening in self-assembled QDs.

2. Theoretical model

2.1. Ladder configuration for EIT operation

A schematic diagram of potential profile and relevant parameters for EIT operation in a QD is shown in figure 1. In this ladder configuration, only $|2\rangle \leftrightarrow |1\rangle$ and $|3\rangle \leftrightarrow |2\rangle$ are dipole-allowed, of which the energy separation is $\hbar\omega_{21}$ and $\hbar\omega_{32}$, respectively. ω_s and ω_p are the optical frequencies of the signal and the pump, respectively. The time-dependent optical dielectric constant experienced by the signal beam can be derived from the density matrix theory as follows.

$$\dot{\rho}_{nm} = -(\mathrm{i}\omega_{nm} + \gamma_{nm}) - \frac{\mathrm{i}}{\hbar}\left[\hat{V}, \hat{\rho}\right]_{nm}, \qquad V_{nm} = -\tfrac{1}{2}\mu_{nm}E(\omega) + \text{c.c.}, \tag{1}$$

where γ_{nm} is the dephasing linewidth, and ω_{nm} is the energy separation between state $|n\rangle$ and $|m\rangle$. μ_{nm} is the dipole moment. The electric field $E(\omega)$ includes the signal and pump beam so that it is expressed as $E(\omega) = E_s e^{-i\omega_s t} + E_p e^{-i\omega_p t}$. When both the signal and pump detunings

are small, we can define the slowly-varying density matrices σ_{nm} as follows.

$$\begin{aligned}\rho_{21}(t) &= \sigma_{21}(t)\mathrm{e}^{-\mathrm{i}(\omega_\mathrm{s})t},\\ \rho_{32}(t) &= \sigma_{32}(t)\mathrm{e}^{-\mathrm{i}(\omega_\mathrm{p})t},\\ \rho_{31}(t) &= \sigma_{31}(t)\mathrm{e}^{-\mathrm{i}(\omega_\mathrm{s}+\omega_\mathrm{p})t}.\end{aligned} \tag{2}$$

The substitution of equation (2) into (1) leads to the equation of motion for σ_{nm} elements. The off-diagonal elements are given by

$$\begin{aligned}\dot{\sigma}_{21} &= -(\gamma_{21}+\mathrm{i}\Delta_\mathrm{s})\sigma_{21} - \mathrm{i}\Omega_\mathrm{s}(\rho_{22}-\rho_{11}) + \mathrm{i}\Omega_\mathrm{p}^*\sigma_{31},\\ \dot{\sigma}_{32} &= -(\gamma_{32}+\mathrm{i}\Delta_\mathrm{p})\sigma_{32} - \mathrm{i}\Omega_\mathrm{p}(\rho_{33}-\rho_{22}) - \mathrm{i}\Omega_\mathrm{s}^*\sigma_{31},\\ \dot{\sigma}_{31} &= -[\gamma_{31}+\mathrm{i}(\Delta_\mathrm{s}+\Delta_\mathrm{p})]\sigma_{31} + \mathrm{i}\Omega_\mathrm{p}\sigma_{21} - \mathrm{i}\Omega_\mathrm{s}\sigma_{32},\end{aligned} \tag{3}$$

where the definition of the Rabi frequency is $\Omega \equiv \mu E/2\hbar$. $\Delta_\mathrm{s} = \omega_{21} - \omega_\mathrm{s}$ and $\Delta_\mathrm{p} = \omega_{32} - \omega_\mathrm{p}$ are detunings from the signal and pump beam, respectively.

The steady-state solution of σ_{31} in equation (3) is

$$\sigma_{31} = \frac{\mathrm{i}(\Omega_\mathrm{p}\sigma_{21} - \Omega_\mathrm{s}\sigma_{32})}{\gamma_{32} + \mathrm{i}\left(\Delta_\mathrm{s}+\Delta_\mathrm{p}\right)}. \tag{4}$$

If we assume that the power of the signal is much smaller than that of the pump, the second term in the numerator can be dropped. In this case, the approximate solution of σ_{21} in equation (3) is expressed as

$$\sigma_{21} = \frac{\mathrm{i}\Omega_\mathrm{s}\,(\rho_{11}-\rho_{22})}{\tilde{\gamma}_{21}\left(1+\frac{|\Omega_\mathrm{p}|^2}{\tilde{\gamma}_{21}\tilde{\gamma}_{31}}\right)}, \tag{5}$$

where $\tilde{\gamma}_{21} = \gamma_{21} + \mathrm{i}\Delta_\mathrm{s}$ and $\tilde{\gamma}_{31} = \gamma_{31} + \mathrm{i}(\Delta_\mathrm{s}+\Delta_\mathrm{p})$. Correspondingly, the first-order optical susceptibility seen by the signal, $\chi(\omega_\mathrm{s})$, is expressed as [1]

$$\begin{aligned}&\chi(\omega_\mathrm{s}) = \chi'(\omega_\mathrm{s}) + \mathrm{i}\chi''(\omega_\mathrm{s}),\\ &\chi'(\omega_\mathrm{s}) = \varepsilon_\mathrm{bac} + \frac{U_{21}}{\hbar}\frac{\gamma_{31}^2\Delta_\mathrm{s} - (\Delta_\mathrm{s}+\Delta_\mathrm{p})[\Omega_\mathrm{pp}^2 - \Delta_\mathrm{s}(\Delta_\mathrm{s}+\Delta_\mathrm{p})]}{[\Omega_\mathrm{pp}^2 + \gamma_{21}\gamma_{31} - \Delta_\mathrm{s}(\Delta_\mathrm{s}+\Delta_\mathrm{p})]^2 + [\gamma_{21}(\Delta_\mathrm{s}+\Delta_\mathrm{p}) + \gamma_{31}\Delta_\mathrm{s}]^2},\\ &\chi''(\omega_\mathrm{s}) = \frac{U_{21}}{\hbar}\frac{\gamma_{31}(\Omega_\mathrm{pp}^2 + \gamma_{21}\gamma_{31}) + \gamma_{21}(\Delta_\mathrm{s}+\Delta_\mathrm{p})^2}{[\Omega_\mathrm{pp}^2 + \gamma_{21}\gamma_{31} - \Delta_\mathrm{s}(\Delta_\mathrm{s}+\Delta_\mathrm{p})]^2 + [\gamma_{21}(\Delta_\mathrm{s}+\Delta_\mathrm{p}) + \gamma_{31}\Delta_\mathrm{s}]^2},\end{aligned} \tag{6}$$

where ε_bac is a background dielectric constant; $U_{21} = (\Gamma/V)|\mu_{21}|^2(f_1 - f_2)/\varepsilon_0$ and $\Omega_\mathrm{pp}^2 = |\mu_{32}|^2 I_\mathrm{p}/4\hbar^2 c\varepsilon_0\sqrt{\varepsilon_\mathrm{bac}}$ are related to the oscillator strength of the signal beam and the launched pump power density, respectively; γ_{21} and γ_{31}, which depend on the homogeneous broadening of QDs, are the damping rates for $|2\rangle \leftrightarrow |1\rangle$ and $|3\rangle \leftrightarrow |1\rangle$ transitions, respectively; Γ is the optical confinement factor; V is the volume of a single QD; μ_{21} and μ_{32} are the interband and intersubband dipole moments, respectively; f_1 and f_2 are Fermi–Dirac occupation factors and for a passive undoped dot, $f_1 \sim 1$ and $f_2 \sim 0$; and ε_0 and c are the dielectric constant and the speed of the light in vacuum, respectively.

The group velocity slow-down factor is defined as the ratio of the light propagation time of the device length to that of free space. When the detunings from the signal and pump beams are zero, the slow-down factor (S) at the signal frequency (ω_s) can be derived from this dielectric constant [3]

$$S = \left[\frac{\varepsilon_\mathrm{bac} + \sqrt{\varepsilon_\mathrm{bac}^2 + \varepsilon_\mathrm{res}^2}}{2}\right]^{1/2}\left[1 + \frac{\hbar\omega_\mathrm{s}}{2\sqrt{\varepsilon_\mathrm{bac}^2 + \varepsilon_\mathrm{res}^2}}\frac{U_{21}(\Omega_\mathrm{pp}^2 - \gamma_{31}^2)}{\hbar^2(\gamma_{31}\gamma_{21} + \Omega_\mathrm{pp}^2)^2}\right], \tag{7}$$

where $\varepsilon_\mathrm{res} = U_{21}/[\hbar(\gamma_{21} + \Omega_\mathrm{pp}^2/\gamma_{31})]$.

2.2. Quantum dot model

We consider a strained GaAs–InGaAs–InAs QD system, which has a ground state emission wavelength near 1.3 μm [10]. In our model, the dot is treated as a quantum disc with a radius a of 9 nm and a height h of 3.5 nm. Band gap shifts due to the biaxial compressive strain are taken into account. The calculated transition wavelengths for the three-level system as shown in figure 1 are 1.36 μm for the C1–HH1 transition, and 12.8 μm for the C2–C1 transition. The wavefunction of the quantum disc is obtained by solving the Schrödinger equation under the parabolic band model. Band mixing between hole states is not considered in this work. Each state can be characterized by three integral quantum numbers (nml), where nm and l correspond to ρ–ϕ (transverse) and z dependence, respectively ($n \geqslant 1$, $m \geqslant 0$, and $l \geqslant 1$). The wavefunction of the state (nml) at the position $\mathbf{r} = (\rho, \phi, z)$ can be expressed as follows.

$$\phi_d(\mathbf{r}) = C_{mn}\frac{\mathrm{e}^{\mathrm{i}m\phi}}{\sqrt{2\pi}}\begin{cases} J_m(p\rho)\cos(k_z z) & \rho \leqslant a \text{ and } |z| \leqslant h/2, \\ J_m(p\rho)\cos(k_z h/2)\mathrm{e}^{-\alpha(|z|-h/2)} & \rho \leqslant a \text{ and } |z| > h/2, \\ \dfrac{J_m(pa)}{K_m(qa)}K_m(q\rho)\cos(k_z z) & \rho > a \text{ and } |z| \leqslant h/2, \\ \dfrac{J_m(pa)}{K_m(qa)}K_m(q\rho)\cos(k_z h/2)\mathrm{e}^{-\alpha(|z|-h/2)} & \text{otherwise.} \end{cases} \quad (8)$$

In equation (8), $J_m(p\rho)$ and $K_m(q\rho)$ are the Bessel function of the first kind and the modified Bessel function of the second kind, respectively; C_{nm} is the normalization constant; and p, q, k_z, and α are constants, which are determined from the boundary conditions at the interface between the quantum disc and the surrounding material.

2.3. Relevant parameters for EIT operation

The intersubband dipole moment between the ground state (C1 or level 2) and the first excited state (C2 or level 3) of the conduction band is given by

$$\mu_{32} = \langle \phi_{d3}(\mathbf{r})|e\mathbf{r}|\phi_{d2}(\mathbf{r})\rangle\,, \quad (9)$$

where e is the unit charge. In our quantum disc model, the wavefunction in equation (8) has a Bessel function dependence in the transverse direction (similar to the LP_{mn} mode of a step-index optical fibre) and a quantum-well-like dependence along the z direction. Figure 2 shows the polarization selection rules of the intersubband dipole moments for quantum discs with different aspect ratios. The first excited state can be either the (111) state or the (102) state depending on the relative magnitude of the radius and the height of the disc. For simplicity, if an infinite potential barrier is assumed, the condition that the energy of the (111) state is lower than the (102) state is given as follows.

$$E_{111} - E_{012} = \frac{\hbar^2}{2m_{\mathrm{e}}^*}\left[\left(\frac{Z_{11}}{a}\right)^2 + \left(\frac{\pi}{h}\right)^2 - \left(\frac{Z_{01}}{a}\right)^2 - \left(\frac{2\pi}{h}\right)^2\right] < 0, \quad (10)$$

which leads to

$$h < 1.82a, \quad (11)$$

where $Z_{11} = 3.8317$ and $Z_{10} = 2.4048$ are the first zeros of the Bessel functions, $J_0(Z_{10}) = 0$ and $J_1(Z_{11}) = 0$, respectively. In other words, when the height of the quantum disc h is smaller than $1.82a$, the first excited state is the (111) state and the z-component of the intersubband dipole moment is zero, as shown in figure 2(a). When $h > 1.82a$, the first excited state is the (102) state and the intersubband dipole moment in the transverse direction vanishes, as shown in figure 2(b). In general, $h < 1.82a$ for a typical quantum dot. Therefore, the polarization

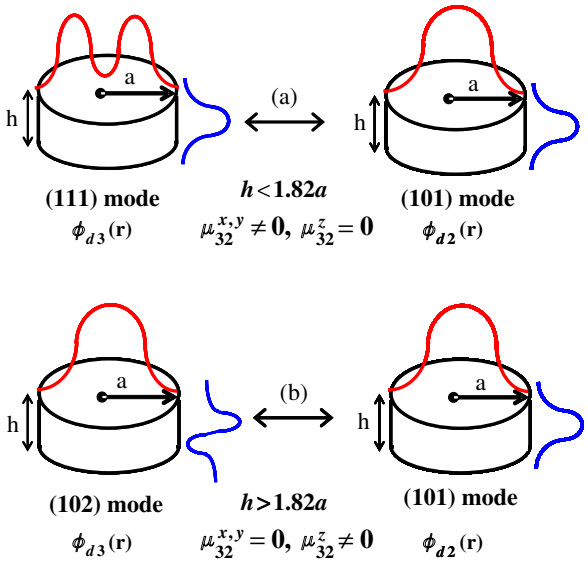

Figure 2. The optical polarization selection rules for the intersubband dipole moment. In (a), the first excited state is the (111)-state and its z-component of the intersubband dipole moment is zero. In (b), the first excited state is the (102)-state and the in-plane (x and y) components of the intersubband dipole moment are zero. We use the convention (nml) that corresponds to quantum numbers in the (ρ, ϕ, z) coordinate system.

of the pump light should be chosen parallel to the QD plane in order to obtain maximum coupling between the pump beam and the $|3\rangle \leftrightarrow |2\rangle$ transition. The calculated intersubband dipole moment in the transverse direction is 24.6 eÅ when the radius and the height are 9 nm and 3.5 nm, respectively. The intersubband dipole moment is proportional to the radius of a QD.

On the other hand, the interband dipole moment can be expressed in terms of the momentum matrix element and the overlap integral of the wavefunctions as follows [11].

$$\mu_{21} = \frac{e}{m_o \omega_s} \xi \, \langle u_c(\mathbf{r})|\mathbf{p}|u_v(\mathbf{r})\rangle \, \langle \phi_{d2}(\mathbf{r})|\phi_{d1}(\mathbf{r})\rangle \,, \tag{12}$$

where $u_c(\mathbf{r})$ and $u_v(\mathbf{r})$ are periodic parts of the ground state for the electron and the hole, respectively; and ξ is an enhancement factor due to excitonic effects; ξ in the range of 41–949 has been reported in CuCl QDs with radii of 15–80 Å embedded in a glass matrix [12]. In the GaAs–InAs–GaAs QD system described above, μ_{21} is calculated to be 5.1 eÅ assuming $\xi = 1$. In the experiment, an interband dipole moment of 21 eÅ was reported in GaAs/AlGaAs QDs [13]. In general, a large interband dipole moment increases the slow-down factor. The value of 21 eÅ will be used below in the calculation of group velocity reduction factor.

The damping rates γ_{21} and γ_{31} are related to the linewidths, or dephasing times, of the QD states, which are determined by several physical processes including radiative recombination, carrier–phonon scattering, and exciton–phonon scatterings, among which the exciton–phonon scattering is considered dominant. The maximum achievable slow-down factor is inversely proportional to the linewidth of a QD [3]. According to the experimental measurement, a single QD has a dephasing time of several tens of picoseconds between 50 and 80 K [14–16].

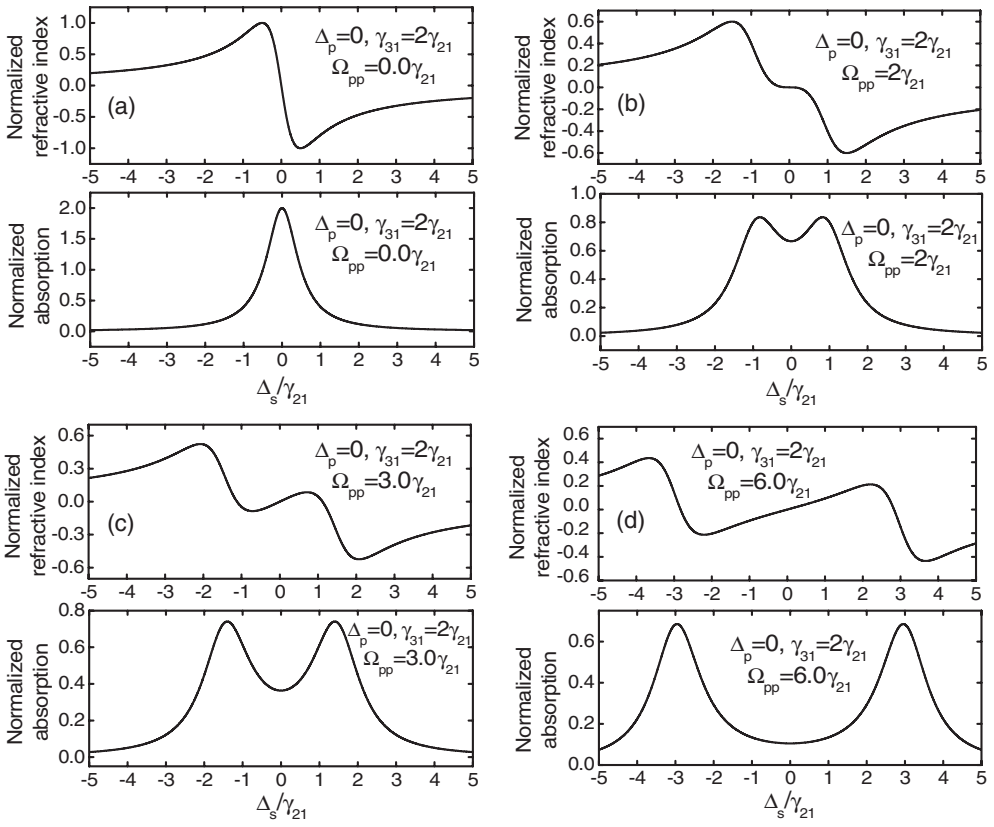

Figure 3. Refractive index (χ') and absorption (χ'') spectra of the normalized first-order susceptibility experienced by the signal beam when the intensity of strong pump beam is varied. γ_{21} is the linewidth of state $|2\rangle$; γ_{31} is the linewidth of state $|3\rangle$; Δ_p is the pump beam detuning; Δ_s is the signal beam detuning; Ω_{pp} is the Rabi frequency of the pump field; $\Delta_p = 0$ and $\gamma_{31} = 2\gamma_{21}$ are assumed; Δ_s and Ω_{pp} are normalized to γ_{21}. (a) $\Omega_{pp} = 0$, (b) $\Omega_{pp} = 2\gamma_{21}$, (c) $\Omega_{pp} = 3\gamma_{21}$, (d) $\Omega_{pp} = 6\gamma_{21}$.

3. Calculation results

Figure 3 shows the variation of the normalized refractive index and absorption spectra from the first-order susceptibility χ_1 of the signal frequency when the intensity of the pump beam is varied [1]. Equation (6) is used to calculate the real and imaginary parts of the susceptibility. In these figures, Δ_p and Δ_s are detuning frequencies for the pump and signal beams, respectively. Ω_{pp} is the Rabi frequency of the pump field. Δ_s and Ω_{pp} are normalized to the linewidth γ_{21}. We assume $\Delta_p = 0$ and $\gamma_{31} = 2\gamma_{21}$ since the excited electron state experiences more dephasing than the ground electron state does. When the pump power density reaches the value of $2\gamma_{21}$ in figure 3(b), the slope of the refractive index (χ') at the centre frequency of the signal beam becomes nearly zero. At the same time, the slow-down factor approaches unity. As we increase the pump power density, the slope of the refractive index spectrum becomes positive and the group velocity starts to decrease. At a certain pump power density, the slope of the refractive index or the group velocity reduction reaches a maximum, as shown in figure 3(c). If the pump power density further increases, the slope of the refractive index starts to decrease again. This is because the increase of the transparency window of the absorption spectrum

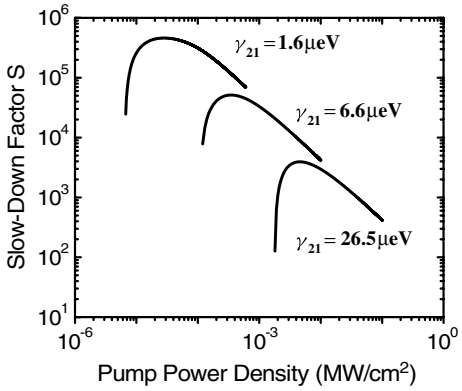

Figure 4. The group velocity slow-down factor is plotted as a function of the pump power density at three linewidth values: $\hbar\gamma_{21}$ is 1.6, 6.6, 26.5 μeV with the assumption $\gamma_{31} = 2\gamma_{21}$.

(χ'') between two absorption peaks experienced by the signal beam reduces the frequency variation of the refractive index profile between the absorption peaks. Therefore, the group velocity reduction due to EIT shows a maximum at a certain pump power density, which agrees with the experimental observation [7]. The bandwidth of an optical buffer via EIT in QDs is determined by the transparency window where the optical absorption is reduced and the slope of the refractive index is positive. As is seen from figure 3(c) in which the maximum group velocity slow-down factor is obtained, the bandwidth is comparable to the linewidth γ_{21}. But the bandwidth can be increased further by increasing the pump power density at the cost of the group velocity slow-down factor, as can be seen from figure 3(d).

The calculated group velocity slow-down factor based on equation (7) is shown in figure 4, using the material parameters defined above. Also, the signal wavelength is 1.36 μm, $\varepsilon_{\text{bac}} = 13$, $|\mu_{21}|/e = 21$ Å, and $|\mu_{32}|/e = 24.6$ Å. Ten vertically-stacked QD layers are used. Each dot has a radius of 9 nm and a height of 3.5 nm. The optical confinement factor, $\Gamma = 6 \times 10^{-3}$ for a QD surface density of 4×10^{10} cm^{-2} is used. Three different linewidth values for $\hbar\gamma_{21}$, 1.6, 6.6, and 26.5 μeV (which correspond to 2.5, 10, and 40 Gbps bandwidths) are considered with the assumption that $\gamma_{31} = 2\gamma_{21}$. The transmission window is determined by the ratio between the Rabi frequency and the linewidth. Figure 4 shows that the calculated group velocity reduction factor for $\gamma_{21} = 26.5$ μeV is around 3000. This reduction factor would be suitable for optical buffers in all-optical packet-switched networks.

4. Quantum dots in a microcavity

The Fabry–Perot cavity structure itself induces slow-down of light by resonant behaviour. Several hundreds of nanoseconds of superluminal (fast light) and subluminal (slow light) propagation was experimentally demonstrated in a high-Q optical microcavity containing a few cold atoms (<10) in its cavity mode [17]. When the EIT effect induced by QDs is incorporated with a resonant cavity, the slow-down factor will increase due to the round-trip behaviour of signal light in the cavity. Hence, we can achieve an enhanced slow-down factor using a smaller number of QDs, which reduces the inhomogeneous broadening effects of QDs. Figure 5 shows a schematic diagram of the QD-microcavity structure. The signal operating wavelength is 1.36 μm and only one layer (instead of ten layers) of QDs is placed at the centre of a λ-cavity. Each of the two distributed Bragg reflectors (DBRs) which form the cavity

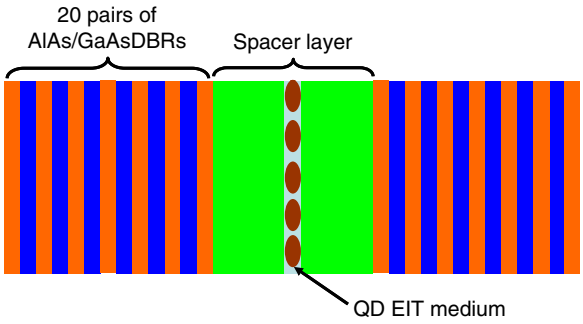

Figure 5. Schematic diagram of the QD-microcavity structure. The respective refractive indices of GaAs and AlAs are 3.5 and 3.1 at $\lambda = 1.36\ \mu$m. The height of the quantum dot is 3.5 nm.

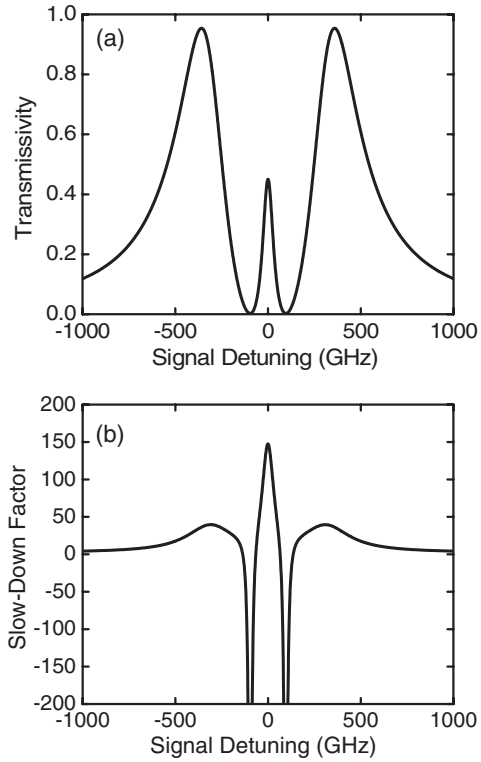

Figure 6. (a) Transmissivity and (b) slow-down factor spectrum of the QD-microcavity when the linewidth of the QDs is 26.5 μeV with the pump beam intensity of 0.1 MW cm^{-2}.

consists of 20 layers of alternating $\lambda/4$ GaAs ($n = 3.5$) and AlAs ($n = 3.1$). The propagation-matrix [18] method is used to obtain the transmission amplitude and phase spectrum. The first-order optical susceptibility induced by EIT is expressed as equation (6). The parameters used for QDs are the same as those in section 3 and only homogeneous broadening of QDs is considered with the assumption that the number of QDs in the centre of the cavity is small. Figure 6 shows the calculated spectrum of transmissivity and slow-down factor through the QD-microcavity when the linewidth ($\hbar\gamma_{21}$) of the QDs is 26.5 μeV with a pump beam intensity

of 0.1 MW cm^{-2}. The slow-down factor induced by only the DBR cavity and the EIT medium is 13 and 18, respectively. Figure 6(b) shows that the slow-down factor caused by the QD-microcavity is around 150. Because the signal experiences multiple round-trips within the cavity, the effective path length increases and the corresponding slow-down factor is enhanced. The optical loss at the centre frequency is 3 dB, as shown in figure 6(a). This enhancement of the slow-down factor by resonance behaviour is limited by the optical loss caused by EIT. If the optical loss induced by EIT is high, the intensities of the multiple reflected signals are negligible and the resonance behaviour disappears.

5. Conclusion

We have theoretically investigated a semiconductor QD system for slow light with applications to a variable semiconductor all-optical buffer. The effects of the dephasing time on the slow-down factor of the signal light are investigated. The main factor of the dephasing is from exciton–phonon scattering, limited by the radiative recombination [15], and it has a value of several tens of picoseconds between 50 and 80 K. At these temperatures, a group velocity slow-down factor of more than 1000 can be obtained, which is appropriate for 40 Gb s^{-1} optical communication systems. A single layer of QDs placed in a microcavity is proposed in order to overcome the degradation of the slow-down factor caused by the inhomogeneous broadening of QDs. Enhancement of the slow-down factor by resonant behaviour is shown by numerical calculation.

Acknowledgment

This work was supported by DARPA under grant number No. AF SA 3631-22549.

References

[1] Marangos J P 1998 *J. Mod. Opt.* **45** 471
[2] Harris S E, Field J E and Imamoglu A 1990 *Phys. Rev. Lett.* **64** 1107
[3] Ku P C, Chang-Hasnain C J and Chuang S L 2002 *Electron. Lett.* **38** 1581
[4] Khurgin J B 2000 *Phys. Rev.* A **62** 013821
[5] Jones D J, Hall K L, Haus H A and Ippen E P 1998 *Opt. Lett.* **23** 177
[6] Phillips D F, Fleischhauer A, Mair A, Walsworth R L and Lukin M D 2001 *Phys. Rev. Lett.* **86** 783
[7] Turukhin A V, Sudarshanam V S, Shahriar M S, Musser J A, Ham B S and Hemmer P R 2002 *Phys. Rev. Lett.* **88** 023602
[8] Fu Y, Ferdos F, Sadeghi M, Wang S M and Larsson A 2002 *J. Appl. Phys.* **92** 3089
[9] Chang-Hasnain C J, Ku P C, Kim J and Chuang S L 2003 *Proc. IEEE* **9** 1884
[10] Yeh N T, Nee T E, Chyi J I, Hsu T M and Huang C C 2000 *Appl. Phys. Lett.* **76** 1567
[11] Chuang S L 1995 *Physics of Optoelectronic Devices* (New York: Wiley) chapter 9
[12] Kataoka T, Tokizaki T and Nakamura A 1993 *Phys. Rev.* B **48** 2815
[13] Guest J R, Stievater T H, Li X, Cheng J, Steel D G, Gammon D, Katzer D S, Park D, Ell C, Thränhardt A, Khitrova G and Gibb H M 2002 *Phys. Rev.* B **65** 241310
[14] Borri P, Langbein W, Schneider S, Woggon U, Sellin R L, Ouyang D and Bimberg D 2001 *Phys. Rev. Lett.* **87** 157401
[15] Bayer M and Forchel A 2002 *Phys. Rev.* B **65** 041308
[16] Kammerer C, Voisin C, Cassabois G, Delalande C, Roussignol P, Klopf F, Reithmaier J P, Forchel A and Gérard J M 1993 *Phys. Rev.* B **66** 041306
[17] Shimizu Y, Shiokawa N, Yamamoto N, Kozuma M, Kuga T, Deng L and Hagley E W 2002 *Phys. Rev. Lett.* **89** 233001
[18] Chuang S L 1995 *Physics of Optoelectronic Devices* (New York: Wiley) chapter 5